Title

Improved Modeling of Canted—Cosine—Theta Magnets

Journal

IEEE Transactions on Applied Superconductivity, 28(3)

ISSN

1051-8223

Authors

Brouwer, L

Arbelaez, D

Caspi, S

et al.

Publication Date

2018

DOI

10.1109/tasc.2017.2775565

Peer reviewed

Improved Modeling of Canted–Cosine–Theta Magnets

L. Brouwer, D. Arbelaez, S. Caspi, M. Marchevsky, and S. Prestemon

***Abstract*—The Canted–Cosine–Theta is a design option for the next generation of high field superconducting dipoles being pursued within the US Magnet Development Program. This paper presents new modeling techniques developed for design and analysis of CCT magnets. For mechanical modeling in ANSYS, three approaches with increasing accuracy are compared: 2-D symmetry models; 3-D periodic symmetry models; and full 3-D models. Methods for the static and transient magnetic simulation using ANSYS are presented with a focus on circuit-coupled models for predicting magnet behavior following quench. Where applicable, simulation results are compared to data from CCT magnet tests at Berkeley.**

***Index Terms*—Accelerator magnets, canted-cosine-theta, high field, superconducting dipole, advanced modeling.**

I. Introduction

THE US Magnet Development Program (US-MDP) is pursuing the Canted-Cosine-Theta (CCT) magnet design as part of a high field superconducting magnet R&D program for high energy physics [1]. This design, first proposed many years ago [2], [3], has more recently been of interest for reducing Lorentz force induced stress in high field Nb_3Sn magnets [4]–[6]. This reduction is achieved by introducing a mechanical structure internal to the winding pack to intercept and prevent the accumulation of Lorentz forces on the level of individual turns [7]. To date, four superconducting CCT magnets above 2 Tesla have been tested at Berkeley reaching bore dipole fields of 2.5, 4.7, 7.4 and 9.1 tesla [8].

First efforts into modeling and analysis of the CCT design focused on magnetics. These studies showed accelerator level field quality is intrinsic and can be obtained without the need for cross section optimization [3], [9]–[11]. In addition, it was demonstrated that higher order and combined function harmonics can be generated by controlling the modulation of the windings [12]. More recently there has been a push towards the development of finite element techniques for mechanical and multiphysics simulation. One first result of this effort was the implementation of models using a 3D periodic symmetry in the windings for straight-section magnetic and mechanical calculations [7], [13], [14].

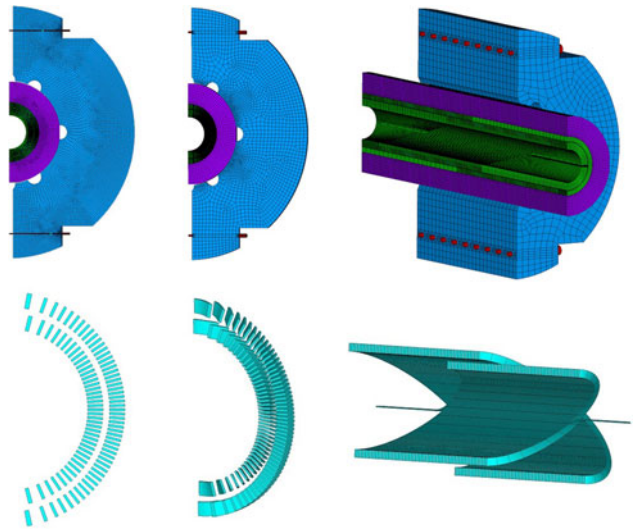

Fig. 1. 2D, 3D periodic, and full 3D ANSYS models for CCT4 are shown with the full structure (top) and the conductor enlarged (bottom).

This paper reviews 2D and 3D periodic mechanical models and presents new full 3D models which include end effects. Assumptions, boundary conditions, and accuracy are discussed, and results are compared with strain gauge measurements from magnet tests at Berkeley. In addition, a new approach which couples both 3D periodic and full 3D finite element models to an external circuit is shown for the modeling of transient magnet behavior after quench. Results from these models and magnet test data are used to show the large effect of structural eddy currents in the protection of CCT magnets.

II. ANSYS Models

A. 2D Models

In traditional accelerator magnet geometries the conductor away from the coil ends is parallel to the axial (length) direction of the magnet. This typically results in a structure similarly unchanging along the length, which allows for use of a 2D symmetry model. This approach simulates behavior far from the ends of a long magnet in what is typically referred to as the "straight-section". CCT windings are 3D in the straight-section (see conductor in Fig. 1 for example), meaning the use of a 2D approach greatly misrepresents the conductor and winding mandrel geometry.

Manuscript received August 28, 2017; accepted October 27, 2017. Date of publication November 20, 2017; date of current version December 14, 2017. This work was supported by the Director, Office of Science, High Energy Physics, and U.S. Department of Energy under contract no. DE-AC02-05 CH11231. *(Corresponding author: L. Brouwer.)*

The authors are with Lawrence Berkeley National Laboratory, Berkeley, CA 94720 USA (e-mail: lnbrouwer@lbl.gov).

Color versions of one or more of the figures in this paper are available online at http://ieeexplore.ieee.org.

Digital Object Identifier 10.1109/TASC.2017.2775565

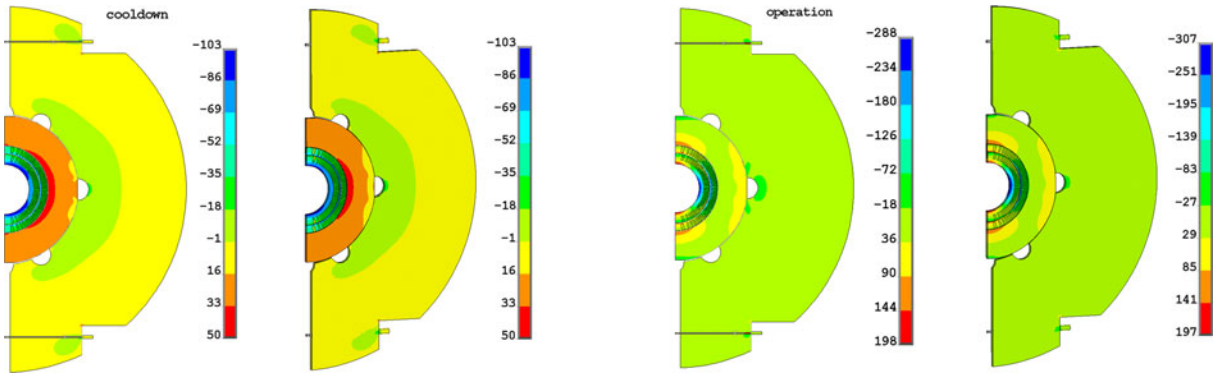

Fig. 2. Azimuthal stress with units of MPa is compared between 2D and 3D periodic plane stress, straight-section models for cooldown (left) and 18.1 kA Lorentz force (right) load steps. More details of the comparison can be found in Table I.

That said, the authors have found 2D CCT models to be useful for studying the behavior of the magnet as a whole. Given quick solution times and relative simplicity of generating and meshing the geometry, 2D approaches can more easily be used for parametric studies. When a more accurate representation of the full conductor stress state is desired one of the more detailed 3D approaches can be used. Section III compares 2D and 3D straight-section models to show 2D models can predict stress in the mandrels and external structure with surprising accuracy.

B. 3D Periodic Models

The minimum axial symmetry of a CCT magnet is a short 3D region with length equal to the pitch of the windings (of the order of 1 cm). This region, seen in the center of Fig. 1, can be used with periodic boundary conditions for straight-section modeling. This is accomplished by using a similar mesh on both axial faces of the region and enforcing constraint equations between like nodes. For mechanical models the displacement degree of freedom is coupled in the transverse plane and related up to a constant in the axial direction. The axial strain constant for different regions of the magnet can be chosen to generalize plane strain, plane stress, and other axial interface behavior to the 3D geometry (for more details see [7]).

For magnetic models a continuous mesh is used throughout the geometry to avoid having to couple the potential across dissimilar mesh interfaces. To avoid transitional elements (pyramids), which create issues during the application of the periodic boundary conditions, a single element type is used. Given the difficulty of meshing the complex geometry with only hexahedral elements a continuous mesh of tetrahedral elements is chosen. For magnetic models using the vector potential degree of freedom the periodicity is enforced by coupling all directions of the vector potential of matching nodes on the two axial surfaces.

For edge elements, like SOLID237, the coupling is more complicated. The edge potential A_z carried by the midside nodes must be coupled with the edge direction considered. In ANSYS the edge direction points from the lower to higher number corner node on the edge where the midside node is found. This is not guaranteed to be consistent for matching nodes on the faces to be coupled, even when the same surface mesh is generated (using MSHCOPY for example). To successfully couple the edge element model, a script compares edge directions for each midside node pair and modifies the constraint equation sign for pairs with opposite edge directions.

C. Full 3D Models

Full 3D models can be used when the influence of end effects on the behavior of the magnet is desired. In this case the full geometry of the conductor and structure is generated and meshed (see right-hand side of Fig. 1). The large number of elements required to mesh the full geometry typically makes the solution of such models beyond the capability of desktop computers. These models have been solved using the LRC Lawrencium cluster at Berkeley. In particular, the use of distributed HPC ANSYS with the PCG solver has shown an order of magnitude reduction in solution time for large mechanical models.

III. Mechanical Modeling for CCT4

During the design of CCT4, 2D, 3D periodic, and full 3D mechanical models were generated and solved (details of the design can be found in [9]). A three load step solution was used including: (1) assembly with yoke rod tension, (2) cooldown to 4.2 K, and (3) powering to 18.1 kA Lorentz forces. In the first load step the yoke rods are pre-tensioned to a stress of 105 MPa which corresponds to the value used for the magnet test. The rod diameter for the 2D and 3D periodic models is scaled to keep the rod area per length the same as full 3D model.

For the 2D model, the Lorentz forces are applied from a previous ANSYS magnetic model solution, and for the 3D models the Lorentz forces are calculated at the element centroids in Opera3D and then transferred to ANSYS. Unless mentioned, the contact condition between layers is sliding with a friction coefficient of 0.2 and isotropic, blended material properties are assumed for the conductor regions with values consistent with what is used in the design of the Nb_3Sn LARP quadrupoles [15], [16].

A. Comparison of Straight-Section Models

The 2D and 3D periodic models both simulate the behavior of a long magnet far from the ends. To compare results between the two approaches, each was solved with a plane stress condition. The results are shown in Fig. 2 and Table I. Fig. 2 compares the azimuthal stress for the cooldown and Lorentz force loads steps, and Table I compares the peak stress in the various

TABLE I
RESULTS COMPARISON BETWEEN 2D AND 3D PERIODIC MODELS

		Bolted Assembly 2D/3D Periodic	Cooldown to 4.4 K 2D/3D Periodic	Operation at 18.1 kA 2D/3D Periodic
Mandrel	σ_θ	−22/−24	−102/−111	−288/−301
	σ_z	0/−6	0/14	0/−85
	von Mises	22/22	102/106	289/314
Conductor	σ_θ	6/6	−40/−28	−77/−83
	σ_z	0/3	0/16	0/35
	von Mises	6/7	41/38	79/103
Shell	σ_θ	−21/−19	44/48	127/125
	σ_z	0/−12	0/−13	0/38
	von Mises	22/13	57/59	128/113

Peak stresses (in MPa) are compared between 2D and 3D plane stress straight-section models. The generalization of plane stress over entire components and the inclusion of 3D forces results in non-zero axial stress in the 3D periodic model. Despite making large simplifications to the geometry and not containing axial Lorentz forces, the results in 2D are similar to those in 3D.

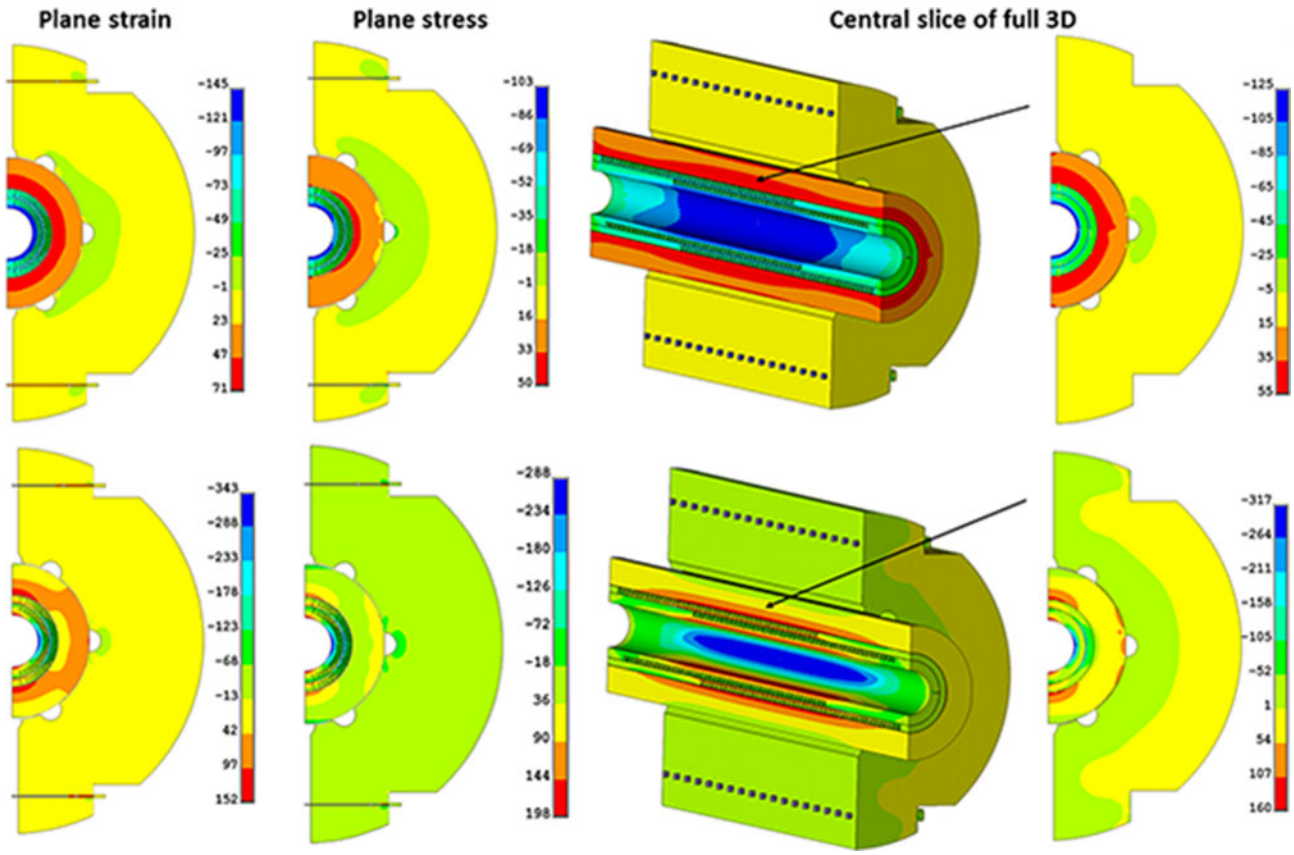

Fig. 3. Azimuthal stress in units of MPa is compared between 2D models with plane stress and plane strain boundary conditions to a central slice of a long full 3D model with friction sliding between layers. Stress is shown for both cooldown (top) and 18.1 kA Lorentz force (bot) load steps. It is seen that the 2D boundary conditions of plane strain and plane stress can be used to bound the expected results of the full 3D model.

components at all load steps. Despite the limited ability of the 2D model to represent the true conductor geometry and axial forces, its results are mostly consistent with those of the 3D periodic model.

B. 2D Boundary Condition Comparison to 3D Full

A full 3D model of CCT4 with physical length doubled from 1 m to 2 m was generated in order to compare results to the straight-section models. The goal of this comparison was to understand whether plane stress or plane strain boundary conditions more accurately models the behavior of a long CCT magnet with friction sliding interfaces between layers. The results of this comparison are shown in Fig. 3. The stresses of the full 3D model are seen falling between the two extremes of plane strain and plane stress, with neither being significantly more accurate than the other. This suggests a valuable role for straight-section

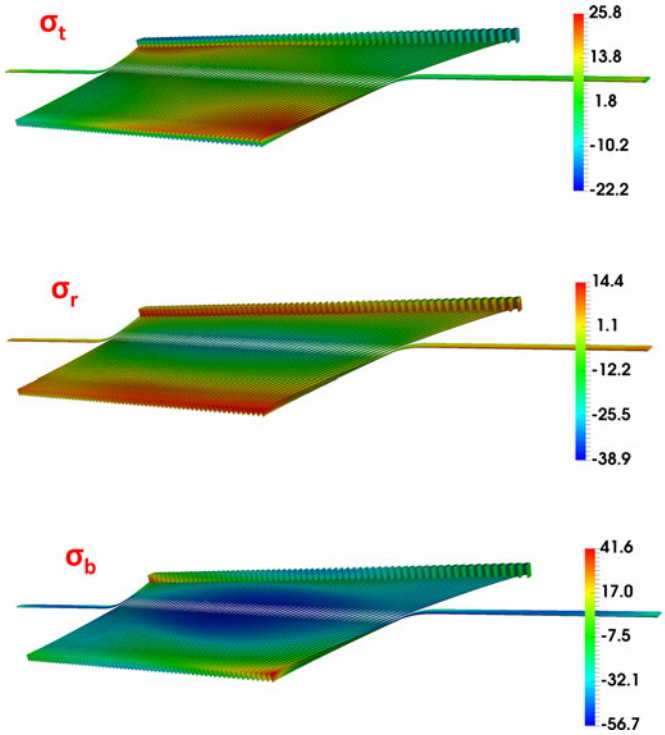

Fig. 4. Local frame normal stresses from the full 3D model are shown for layer 1 of CCT4 at the final load step with 18.1 kA Lorentz force.

TABLE II
LOCAL FRAME CONDUCTOR STRESS: FULL 3D MODEL (IN MPA)

	Cooldown to 4.4 K	Operation at 18.1 kA
σ_t (min/max)	−29/13	−22/26
σ_r	−10/9	−39/14
σ_b	−77/−21	−57/42
σ_{tr}	−2/1	−10/8
σ_{rb}	−8/14	−34/14
σ_{tb}	−7/11	−35/35

models, which is to bound the expected behavior in 3D with a simplified geometry and a greatly reduced number of elements.

C. CCT4 Conductor Stress in a Local Frame

The strain sensitivity of Nb_3Sn motivates effort into a detailed study of the stress state of the conductor. For this, results from the full and periodic 3D models for CCT4 were transformed into a reference frame local to the cable. This frame changes along the length of the path such that $\hat{t}$ is directed tangent to the conductor, $\hat{r}$ is radial, and $\hat{b}$ completes the frame with a direction perpendicular to the rib (and the broad face of the cable). Fig. 4 shows the three normal stresses in the final load step, and Table II lists the peak of all the components for both cooldown and operation. It is seen that all conductor stresses are well below accepted conductor stress limits of 150–200 MPa, and also that powering the magnet produces large shear between the cable and mandrel channels (up to 35 MPa). This shear at an epoxy held interface has been identified as a potential source of

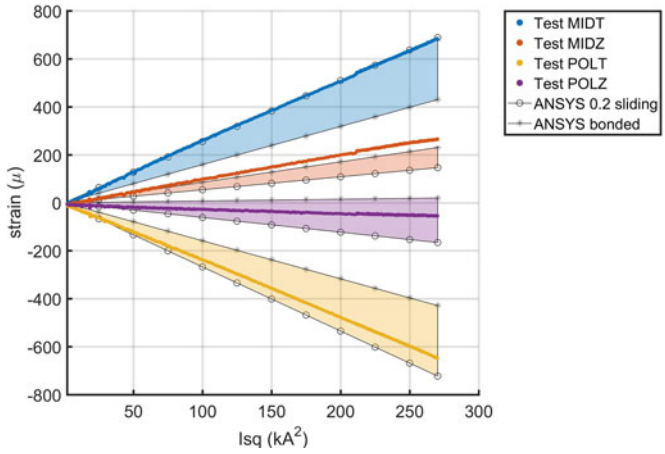

Fig. 5. Strain gauge measurements at the pole (POL) and midplane (MID) in the azimuthal (T) and axial (Z) directions are compared to a range of values predicted by ANSYS models during magnet powering. The range is bounded by ANSYS results with bonded and friction sliding interfaces between layers. General agreement between the ANSYS modeling and measurements is seen, with the results being closer to friction sliding.

TABLE III
COMPARISON OF COOLDOWN SHELL STRAIN (IN μ)

	POLT	POLZ	MIDT	MIDZ
CCT4 test meas.	216	193	233	222
ANSYS friction	275	214	259	230
ANSYS bonded	281	261	288	267

training for CCT magnets which will be further explored with modeling and magnet test diagnostics.

D. Comparison to Strain Gauge Data

CCT4 was instrumented with strain gauges on the outer diameter of the aluminum shell at the location of the axial center of the magnet. Stations were placed to measure azimuthal and axial strain at both the pole and midplane. Measurements taken by these gauges were compared to results from the full 3D ANSYS model of the CCT4. One difference between CCT3 and CCT4 was the implementation of slip planes between layers during epoxy impregnation [9].

In an attempt to understand the effectiveness of this, an ANSYS model with bonding between layers was also solved to give a range of expected strain between the two cases. A comparison of this range to the strain gauge measurements during a current ramp is shown in Fig. 5, and the cooldown strain is compared in Table III. The predicted and measured strain agree reasonably well, with both the powering and cooldown measurements tending towards the ANSYS model with friction sliding.

IV. CIRCUIT COUPLED MAGNETIC MODELS IN ANSYS

The conductor of CCT4 is surrounded by aluminum bronze winding mandrels, and outside of these mandrels is a large aluminum shell. An approach to modeling eddy currents induced in these structures was developed in ANSYS to begin the study

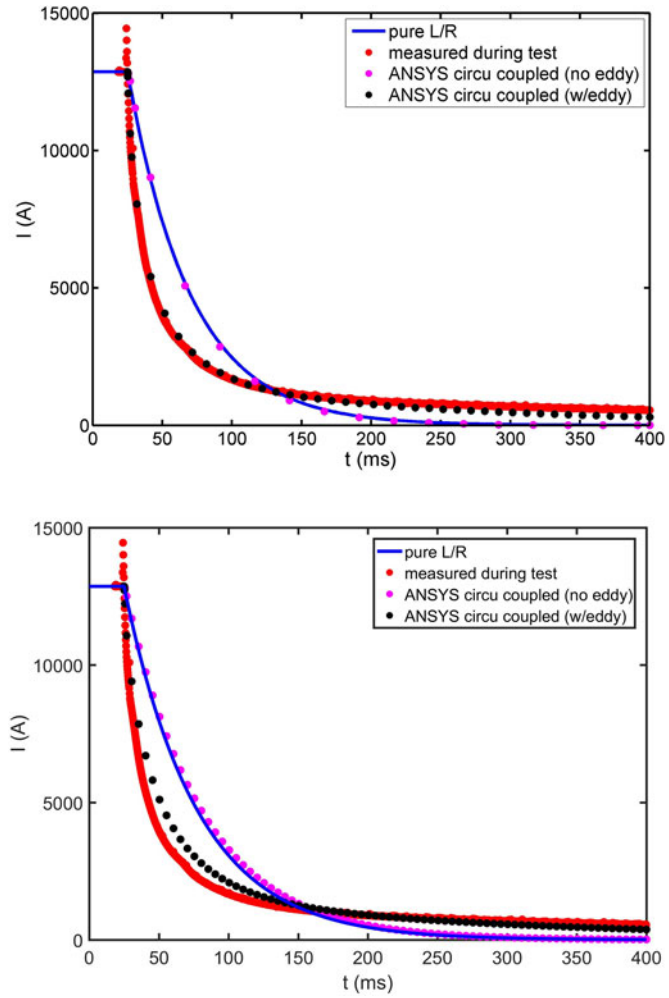

Fig. 6. ANSYS circuit coupled simulations for full 3D (top) and 3D periodic (bot) models are compared to measured current decay during test. Energy deposition for the various decays are given in Table IV.

of how these eddy currents affect magnet protection. As a first step towards this goal, periodic and full 3D magnetic ANSYS models were created and bench marked with Opera3D for accuracy. The 3D periodic model uses Solid237 magnetic edge elements and the full 3D model uses Solid97 nodal vector potential elements. While the edge potential would be desirable for both models, the total potential is chosen for the full 3D case due to it having several dissimilar mesh interfaces which arise from using a mixed quadrilateral and tetrahedral mesh. In this case the continuity of the total potential can be enforced with commands internal to ANSYS (CEINTF) without the need for custom scripts to include edge direction. Also, given the orientation of the flux with respect to the iron, it also expected that the total potential will be accurate for this geometry.

A method was developed to couple the finite element regions of these models to an external circuit within ANSYS using CIRCU124 elements. With this approach, the effect of eddy currents in the magnet structure can be coupled to the behavior of the magnet in the circuit. Future work will focus on including losses within the cable and growth of a resistance zone to capture other contributions to the decay not included in this analysis

TABLE IV
ENERGY DISSIPATION DURING MAGNET DECAY

	MIITS	Edump(kJ,%)	Eshell(kJ,%)	Eman(kJ,%)
ANSYS Full (no ed.)	3.76	150, 100%	0	0
ANSYS Full (eddy)	1.80	72, 47%	70, 46%	7, 5%
ANSYS Per. (no ed.)	4.58	173, 100%	0	0
ANSYS Per. (eddy)	2.38	96, 55%	72, 41%	4, 3%
Test measurement	1.78	71, 47%	unknown	unknown

(which, for example, would be critical for modeling protection with CLIQ [17]).

Fig. 6 shows simulation results for current decay post quench compared to test data for both 3D periodic and full 3D models. In each case, the FEA region is coupled to a circuit representing a simplified version of the Magnet Test Facility at Berkeley. The simulation is started with the peak current, and the decay is simulated with no assumptions of the inductance or other magnet losses. Energy losses in this case occur only in the dump resistor of the external circuit and the magnet structure.

Table IV lists the energy lost by each mechanism for both the test and ANSYS data. As a check, each ANSYS simulation was also run once without eddy currents to verify the coupling of the magnet to an external circuit for a simple L/R case. It is seen that the eddy currents in the structure play a significant role in the protection by drastically increasing the speed of the magnet current decay. As a result the MIITS is nearly halved, with 50% of the stored energy being deposited in structural eddy currents. From the table it is seen that the majority of the losses occur in the aluminum shell, which can be explained by its lower resistivity and larger size with respect to the aluminum bronze winding mandrels.

Both models fairly accurately predict the large deviation from L/R decay seen in the test data. The underestimation of the decay speed could be due to the missing contributions of conductor losses and resistance growth which are not yet implemented in the simulation. While the full 3D model shows better agreement to test data (includes end effects), the results of the 3D periodic model show promise to be accurate enough for parametric studies with an order of magnitude reduction in number of mesh elements.

V. CONCLUSION

New methods for mechanical and magnetic modeling of CCT magnets were presented. Accuracy and boundary conditions were compared between 2D, 3D periodic, and full 3D mechanical models to validate the approach and gain understanding of the usefulness of each. Details of the conductor stress for CCT4 were given, and agreement between full 3D ANSYS models and shell strain gauge measurements taken during the CCT4 test was shown. Finally, magnet current decay measured during the test was compared to results from circuit coupled, transient magnetic models in ANSYS. The simulations and test data indicate eddy currents in the aluminum shell of CCT4 play a large role in magnet protection by increasing the speed of magnet current decay. These effects were shown reducing the MIITS by up to a factor of two.

REFERENCES

[1] S. Gourlay, S. Prestemon, A. Zlobin, L. Cooley, and D. Larbalestier, "The U.S. magnet development program plan," Lawrence Berkeley Nat. Lab., Berkeley, CA, USA, 2016. [Online]. Available: https://www.osti.gov/scitech/servlets/purl/1306334

[2] D. Meyer and R. Flasck, "A new configuration for a dipole magnet for use in high energy physics applications," *Nucl. Instr. Meth. Phys. Res. A*, vol. 80, no. 2, pp. 339–341, 1970.

[3] C. Goodzeit, M. Ball, and R. Meinke, "The double-helix dipole—A novel approach to accelerator magnet design," *IEEE Trans. Appl. Supercond.*, vol. 13, no. 2, pp. 1365–1378, Jun. 2003.

[4] S. Caspi *et al.*, "The canted-cosine-theta magnet (CCT)—A concept for high field accelerator magnets," *IEEE Trans. Appl. Supercond.*, vol. 24, no. 3, Jun. 2014, Art. no. 4001804.

[5] S. Caspi, D. Arbelaez, L. Brouwer, S. Gourlay, S. Prestemon, and B. Auchmann, "Design of a canted-cosine-theta superconducting dipole magnet for future colliders," *IEEE Trans. Appl. Supercond.*, vol. 27, no. 4, Jun. 2017, Art. no. 4001505.

[6] B. Auchmann *et al.*, "Electromechanical design of a 16-T CCT twin-aperture dipole for FCC," *IEEE Trans. Appl. Supercond.*, to be published.

[7] L. Brouwer, D. Arbelaez, S. Caspi, H. Felice, S. Prestemon, and E. Rochepault, "Structural design and analysis of canted-cosine-theta dipoles," *IEEE Trans. Appl. Supercond.*, vol. 24, no. 3, Jun. 2014, Art. no. 4001506.

[8] S. Caspi *et al.*, "Test results of CCT1–A 2.4t canted-cosine-theta dipole magnet," *IEEE Trans. Appl. Supercond.*, vol. 25, no. 3, Jun. 2015, Art. no. 4002304.

[9] A. V. Gavrilin, M. D. Bird, V. E. Keilin, and A. V. Dudarev, "New concepts in transverse field magnet design," *IEEE Trans. Appl. Supercond.*, vol. 13, no. 2, pp. 1213–1216, Jun. 2003.

[10] S. Caspi *et al.*, "Design, fabrication, and test of a superconducting dipole magnet based on tilted solenoids," *IEEE Trans. Appl. Supercond.*, vol. 17, no. 2, pp. 2266–2269, Jun. 2007.

[11] S. Farinon and P. Fabbricatore, "Refined modeling of superconducting double helical coils using finite element analyses," *Supercond. Sci. Technol.*, vol. 25, no. 6, 2012, Art. no. 065006.

[12] C. Goodzeit, R. Meinke, and M. Ball, "Combined function magnets using double-helix coils," in *Proc. Particle Accelerator Conf.*, 2007, pp. 560–562.

[13] S. Caspi *et al.*, "A superconducting magnet mandrel with minimum symmetry laminations for proton therapy," *Nucl. Instr. Meth. Phys. Res. A*, vol. 719, pp. 44–49, 2013.

[14] G. Montenero *et al.*, "Mechanical structure for the psi canted-cosine-theta (CCT) magnet program," presented at the 25th Int. Conf. Magn. Technol., Amsterdam, The Netherlands, 2017.

[15] H. Pan *et al.*, "Assembly tests of the first Nb3Sn low-beta quadrupole short model for the hi-LUMI LHC," *IEEE Trans. Appl. Supercond.*, vol. 26, no. 4, Jun. 2016, Art. no. 4001705.

[16] G. Vallone *et al.*, "Mechanical performance of the short models for MQXF, the Nb3Sn low-beta quadrupole for the Hi-Lumi LHC," *IEEE Trans. Appl. Supercond.*, vol. 27, no. 4, Jun. 2017, Art. no. 4002906.

[17] E. Ravaioli, "Cliq. A new quench protection technology for superconducting magnets," Ph.D. dissertation, Univ. Twente, Enschede, The Netherlands, 2015.